View metadata, citation and similar papers at core.ac.uk
brought to you by CORE
provided by Gutenberg Open

Role of the magnetic anisotropy on the spin configurations of patterned $La_{0.7}Sr_{0.3}MnO_3$ elements

P. Wohlhüter,[1,2,3] J. Rhensius,[1,4] C. A. F. Vaz,[2,5,*] J. Heidler,[2,3] H. S. Körner,[1,2,3] A. Bisig,[1,2,3] M. Foerster,[5] L. Méchin,[6] F. Gaucher,[6] A. Locatelli,[7] M. A. Niño,[7] S. El Moussaoui,[8] F. Nolting,[8] E. Goering,[9] L. J. Heyderman,[4,10] and M. Kläui[1,2,3,5]

[1] *Fachbereich Physik, Universität Konstanz, Universitätsstraße 10, 78457 Konstanz, Germany*
[2] *SwissFEL, Paul Scherrer Institut, 5232 Villigen PSI, Switzerland*
[3] *Laboratory for Nanomagnetism and Spin Dynamics, Ecole Polytechnique Fédérale de Lausanne (EPFL), 1015 Lausanne, Switzerland*
[4] *Laboratory for Micro- and Nanotechnology, Paul Scherrer Institut, 5232 Villigen PSI, Switzerland*
[5] *Institut für Physik, Johannes Gutenberg-Universität, 55099 Mainz, Germany*
[6] *GREYC, UMR 6072, CNRS - ENSICAEN - UCBN, 6, Boulevard du Maréchal Juin, 14050 Caen Cedex, France*
[7] *Sincrotrone Trieste, 34149 Basovizza-Trieste, Italy*
[8] *Swiss Light Source, Paul Scherrer Institut, 5232 Villigen PSI, Switzerland*
[9] *Max-Planck-Institut für Metallforschung, Heisenbergstrasse 3, 70569 Stuttgart, Germany*
[10] *Mesoscopic Systems, ETH Zürich - Paul Scherrer Institut, 5232 Villigen PSI, Switzerland*

(Dated: February 26, 2013)

We study the effect of magnetocrystalline anisotropy on the magnetic spin configurations of $La_{0.7}Sr_{0.3}MnO_3$ bar and triangle elements using direct photoemission electron microscopy imaging. The dominant remanent state is a low energy flux-closure state for both thin (15 nm) and thick (50 nm) elements. The magnetocrystalline anisotropy, which competes with the dipolar energy, strongly modifies the spin configuration in the thin elements depending on the shape, size and orientation of the structures. We investigate the magnetic switching processes and observe in triangular shaped elements a displacement of the vortex core along the easy axis for an external magnetic field applied along the [100] direction, which is well reproduced by micromagnetic simulations.

I. INTRODUCTION

The colossal magnetoresistance (CMR) manganites are a prototypical class of complex oxide materials, where the strong electron interactions give rise to a large range of physical behavior, including the CMR effect, metal to insulator transitions, and magnetic and orbital order [1–4]. Although studied for several decades now, the recent advances in growth and nanoscale fabrication techniques have allowed for the design and fabrication of new heterostructures where novel functionalities emerge as a consequence of proximity effects or reduced dimensionality [5, 6]. Examples are the recent demonstrations of a large magnetoelectric coupling when a ferromagnetic manganite is interfaced with a ferroelectric layer [7–10] or the coupling of a thin manganite film to the soft phonon modes of $SrTiO_3(001)$, which induces large changes in the electric and magnetic response of the system [11].

To use such magnetic materials in devices, the spin structure needs to be controllable on the nanoscale. Mainly, the element geometry is tailored to achieve the desired spin structure. In particular, at reduced lateral dimensions, the size confinement leads to a reduction in the number of energetically favorable states, as a consequence of the fine interplay between the governing micromagnetic energy terms [12, 13]. Confined spin structures that have raised significant interest in recent years include domain walls and vortices, since they constitute the smallest magnetic spin structure in soft magnetic materials [14]. Also simple physical geometries tend to favor simple magnetic states, such as the vortex state in discs or the Landau state in squares, which combine domain walls and vortices and have been observed in small metallic ferromagnetic elements [14, 15]. It has been shown recently that, despite the complexity inherent to the doped manganites, $La_{0.7}Sr_{0.3}MnO_3$ elements are characterized by simple magnetic states, which are topologically compatible with the shape of the element, showing that the magnetic state can be tailored by suitable choice of the geometry [16, 17].

Apart from the geometrical shape, an additional degree of freedom to manipulate the spin structure is the magnetic anisotropy. For instance, magnetocrystalline anisotropy has been shown to strongly modify the spin structure in metallic ferromagnetic elements [13]. While the influence of the magnetic anisotropies have been studied in metallic structures, the role of the magnetic anisotropy in oxide nanostructures has been studied in much less detail. However, with the prospect of exploring doped manganites for device applications including nanostructures or for the investigation of phenomena appearing at reduced dimensions, special consideration needs to be given to this physical parameter, since one needs to ascertain its influence on the local spin configuration of the system. Of particular importance in determining the strength of the magnetic anisotropy are the roles of the epitaxial strain in single crystalline

* Corresponding author: carlos.vaz@cantab.net

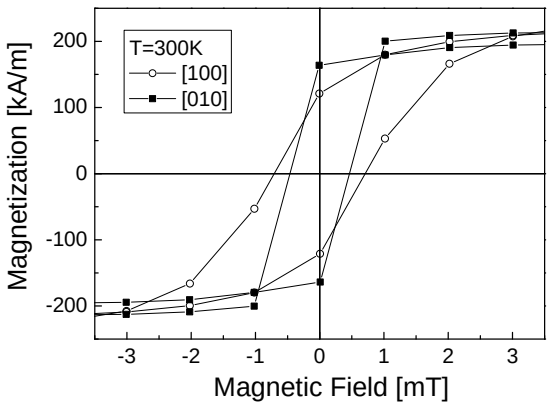

FIG. 1. Magnetic hysteresis loops of a continuous 15 nm thick LSMO film measured by SQUID magnetometry with the field applied along orthogonal <100> azimuths. The change of the coercive field and remanent magnetization points to the presence of a uniaxial anisotropy with the easy axis along the [010] direction.

structures [18–20], of the surface morphology, including atomic steps [21, 22], and of the film orientation with respect to the crystallographic axes [23]. For example, $La_{0.7}Sr_{0.3}MnO_3$ films grown under tensile strain on $SrTiO_3$(001) are magnetized in-plane, while out-of-plane magnetization is favored when grown under compressive strain on $LaAlO_3$(001) surfaces [19, 20]. However, while the role of the magnetic anisotropy has been studied in continuous films, information on the influence of anisotropies on nanoscale spin structures and reversal processes in manganite nanostructures with the most relevant geometries still needs to be obtained in detail.

In this work, we report the results of a study aimed at elucidating the role of the magnetic anisotropy on the magnetic spin configuration of $La_{0.7}Sr_{0.3}MnO_3$ (LSMO) elements using X-ray magnetic circular dichroism photoemission electron microscopy (XMCD-PEEM). In particular we use triangular geometries that are not commensurate with the magnetocrystalline anisotropy symmetry to enhance its effect on the spin structure and on the vortex core. We find that, although comparably weak, a step-induced magnetic anisotropy present in the thin LSMO films gives rise to conspicuous features in the magnetic states of thin $La_{0.7}Sr_{0.3}MnO_3/SrTiO_3$(001) elements. Beyond the equilibrium spin structures, we have studied also the switching process in triangles by directly imaging the magnetic state under an applied magnetic field, allowing us to obtain a detailed picture of the magnetic reversal process, which takes place by domain wall and vortex core displacements and annihilation.

II. SAMPLE GROWTH AND CHARACTERIZATION

The LSMO films were deposited by pulsed laser deposition from a stoichiometric target onto $SrTiO_3$(001) (STO) single crystal substrates. Superconducting quantum interference device (SQUID) magnetometry shows an in-plane magnetization with a Curie temperature (T_c) of about 340 K [17]. Due to the high temperature required for LSMO film growth, ordinary lift-off techniques, e.g. with PMMA, cannot be applied. Therefore for this work, the LSMO films were patterned using a focused ion beam (FIB) [17]. In this technique, the Ga ions implanted in the LSMO cause local structural changes forming non-magnetic areas. This effect is used to write non-ferromagnetic lines that delineate and define the elements.

To determine the effective magnetocrystalline anisotropy, SQUID magnetometry measurements on a 15 nm thick film were performed along orthogonal directions ([100] and [010]) as shown in Fig. 1. It is expected that LSMO has a fourfold magnetocrystalline anisotropy. However, one direction dominates showing the presence of a uniaxial magnetocrystalline anisotropy contribution, which we attribute to step edges [24]. The measurement along the [100] direction shows a larger coercive field and lower remanent magnetization than the [010] direction. The sharper switching along [010] versus [100] is an indication for the existence of a magnetic easy axis oriented close to the [010] direction. Micromagnetic simulations for the study of a triangular structure in applied fields (see Fig. 5) showed best agreement for an orientation of the magnetic easy axis approximately 27° to the [010] direction. Therefore, we assume the magnetic easy axis to be oriented approximately 27° f the [010] direction.

XMCD-PEEM imaging was used to map the magnetic configuration of the elements. In this technique, the local difference in light absorption at resonance for left and right circularly polarized light is probed. The contrast depends on the relative orientation of the magnetization and the X-ray polarization, being maximum for parallel and minimum for anti-parallel alignment. The grazing angle of incidence of the photon beam leads to a high sensitivity of the in-plane component of the magnetization. The images presented here were taken at room temperature at the Mn L_2 edge, at which higher intensity is obtained than at the L_3 edge. XMCD is an element specific effect and ideally suited to investigate the spin configuration of magnetic specimen, since it allows studies without interaction between sample and probing tool. For our measurements, a sample holder containing a Cu coil was used, which allowed in situ application of magnetic fields at the sample position during imaging. Distortions were corrected with the microscope lenses. The experiments were performed at the PEEM endstation of the SIM beamline at the Swiss Light Source and at the Nanospectroscopy beamline at the Elettra-Sincrotrone Trieste. Both microscopes provide spatial resolutions down to 30 nm.

For the 2D micromagnetic simulations, the OOMMF package [25] was used. From the SQUID data, we obtain a saturation magnetization $M_s = 200\,\mathrm{kA/m}$ at

room temperature and a saturation field of about 2 mT, from which we estimate a uniaxial anisotropy of the order of 170 J/m^3; the exchange constant used is $A = 1.5 \times 10^{-12}$ J/m and the in-plane cell size used is 5 nm. Despite slight discrepancies between simulation and experiment, the good agreement allows a qualitative prediction of magnetic states in LSMO elements by micromagnetic simulations.

III. EFFECT OF THE MAGNETOCRYSTALLINE ANISOTROPY ON THE MAGNETIC STATE

The shape of the patterned elements was chosen to allow for the investigation of the effect of the shape and effective magnetocrystalline anisotropy on the magnetic state and to determine the domain and domain wall configurations in LSMO thin film structures. The patterns used consist of basic shapes (triangles, squares and rectangles), which are varied in size and include rotated elements (by 45° and 90°) to study the effect of changing the orientation of the elements with respect to the anisotropy axes on the magnetic configuration. Triangles with one edge aligned close to the magnetic easy axis are expected to have a distorted Landau state, while in bar elements the magnetic configuration should depend on the balance between the effective magnetocrystalline and shape anisotropy, since the spins preferably align along the magnetic easy axis.

A. Square and Rectangular Elements

The influence of the uniaxial anisotropy on the spin configuration is investigated in bar elements of different sizes and thicknesses. The XMCD-PEEM images in Fig. 2 show representative flux-closure Landau states after initial saturation of the sample (along the directions indicated). While ideal Landau states prevail in the 50 nm thick squares [Fig. 2(b)], the 15 nm thin structures [Fig. 2(a)] show that the effective magnetocrystalline anisotropy leads to a Landau state that is asymmetric with the domains in which the spins point parallel to the [010] direction being larger. This is even the case in smaller elements, despite the fact that the shape anisotropy plays a more pronounced role. These differences between the magnetic state of the 15 nm thin and the 50 nm thick squares reflect the importance of the step-induced anisotropy for the resulting spin structure. In Fig. 2(c) XMCD-PEEM images of 15 nm thin rectangular elements are presented. They exhibit flux-closure states, but here the influence of the effective magnetocrystalline anisotropy is very conspicuous. An initial magnetic field along the short edge of the rectangle favors the formation of diamond states [26]. In the rectangles rotated by 90°, a strongly distorted flux-closure four domain state is observed, including the displacement of the vortex cores and antivortices from the expected position, and a larger size of the domains pointing closer to the easy axis. In contrast, the 50 nm thick rectangular structures show well-shaped Landau states without distinct distortions suggesting that the role of the effective magnetocrystalline anisotropy decreases with film thickness [Fig. 2(d)]. This is a consequence of the fact that the magnetostatic energy, which scales with the square of the thickness for in-plane magnetized elements, dominates at larger thicknesses over the magnetocrystalline anisotropy energy, which increases only linearly with the thickness of the element. The observed magnetic states are similar to those found in 3d transition ferromagnetic elements [14, 27, 28], showing that optimally doped LSMO elements follow similar micromagnetic energetics as the 3d metallic counterparts. This is surprising, given the presence of epitaxial strain and the tendency of these complex oxides to exhibit competing electronic phases [1–4].

In elements with edges that make an angle of 45° with respect to the sample edges a similar offset of the vortex core is observed in many elements. In general, the domain configurations of rotated elements (Fig. 3) are more complex than those of the unrotated ones (Fig. 2). The domain states, presented in Fig. 3, are remanent states after the sample was cooled down from a temperature above T_c, which leads to a random initial state. Such complex domain configurations can be stabilized by pinning sites and/or edge roughness. Additionally, they might also be stabilized by the intricate spin structure, i.e., by the interplay between small vortices in the corners of the element and the center vortex. The edge vortices might be stable in this material because of the smaller exchange constant, as well as a uniaxial anisotropy, compared to common 3d ferromagnetic metals.

In Fig. 3(a), a non-centered vortex core in a 2.2 μm large square element is visible in a flux-closure state. The existence of a flux-closure spin structure is primarily determined by the dimension of the element and the

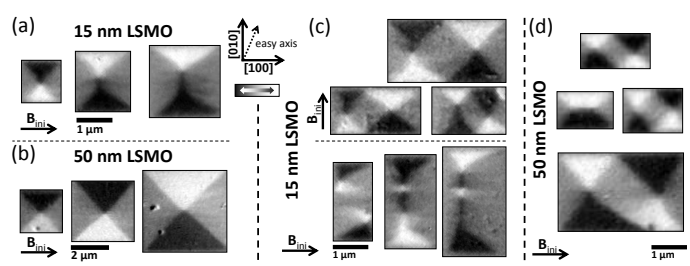

FIG. 2. Domain states in 15 nm and 50 nm thick LSMO bar elements. On the left, square elements of different thicknesses are compared. For the 15 nm thin structures in (a) the Landau state is distorted due to the effective magnetocrystalline anisotropy, whereas non-distorted Landau states are present in the 50 nm thick squares (b). (c) shows rectangular structures of 15 nm thickness. Note the different direction of the initial saturation field in the top and bottom panels. The Landau states of the 50 nm thick rectangles in (d) exhibit effective magnetocrystalline anisotropy-induced distortion.

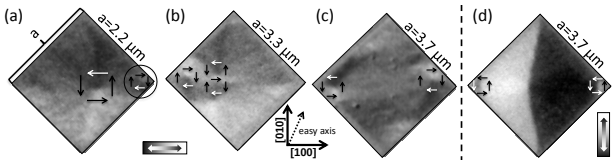

FIG. 3. Examples of XMCD-PEEM images of complex domain structures in 15 nm (a-c) and 50 nm (d) thick, rotated LSMO square elements. In (a), the vortex core is off-center, which we relate to the formation of a small vortex in the adjacent corner (highlighted by a circle). (b) shows a triple vortex configuration in the left hand corner; in (c) and (d) there are two vortex cores in opposite corners (left and right-most corners) minimizing the stray field energy at these positions. Note that the contrast in (a-c) is sensitive to the magnetization along the horizontal direction, while it is sensitive to the vertical direction in (d). The arrows indicate the vortex chirality.

material parameters, but also depends on the field and thermal history of the element. In this image, one can see a small second vortex in the right corner (marked by a circle) with a chirality opposite to that of the large vortex in the center. The existence of the small vortex stabilizes the off-center position of the center vortex. The chirality can be determined from the position of the black and white domains. In Fig. 3(b) a 3.3 μm sized square is depicted. A more complex, stable triple vortex state including an antivortex is observed, demonstrating the reduced influence of the shape anisotropy. Two XMCD images of 3.7 μm elements with different thicknesses are presented in Fig. 3(c) and (d), showing two small vortices that are placed at two diagonally opposite corners. The magnetic easy axis forces the spins to be aligned near the [010] axis and only in the two corners on the left and right hand side the stray field energy can be reduced by the formation of a vortex. Although the elements have different material thicknesses, 15 nm and 50 nm, respectively, the behavior is similar.

B. Triangular Elements

In order to further elucidate the role of the uniaxial anisotropy and the element orientation, we patterned equilateral triangles with edge lengths varying from 1.6 μm to 3.5 μm in a 15 nm thick LSMO film. This geometry allows us to align one edge close to the magnetic easy axis, while the other two edges point at angles that correspond neither to an easy nor to a hard axis. The spin configuration of a flux-closure Landau state in such a triangle depends on the orientation of the element with respect to the crystal axes. Representative XMCD images of triangles of different sizes are presented in the top part of Fig. 4. The domains with magnetization aligned closer to the easy axis ([010]-direction) are dominant, pushing the vortex core to the right (relative to the center). This behavior can also be seen in the corresponding micromagnetic simulations (bottom part of Fig. 4). The relative position of the vortex core depends therefore on the size of the element: the larger the element, the greater is the relative vortex core displacement.

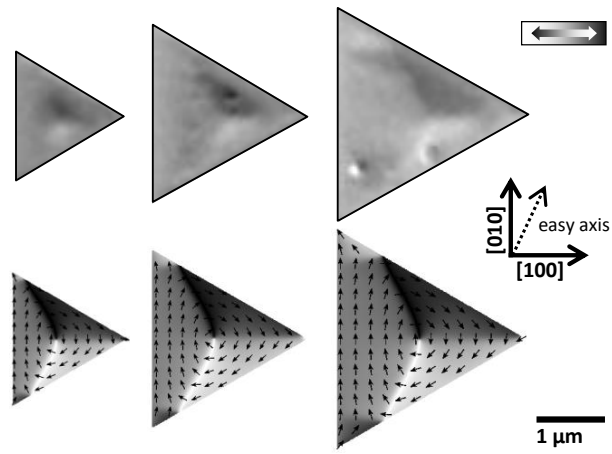

FIG. 4. *Top:* XMCD images of 15 nm thin equilateral LSMO triangles. The magnetic easy axis points in the [010] direction and forces the vortices to be displaced along the hard axis ([100] direction). *Bottom:* Corresponding micromagnetic simulations.

IV. INFLUENCE OF MAGNETIC FIELDS ON THE SPIN CONFIGURATION IN TRIANGULAR ELEMENTS

On application of an external magnetic field, the Zeeman energy leads to changes in the magnetic state. To investigate the influence of the effective magnetocrystalline anisotropy during this process, XMCD-PEEM images of triangles were taken in the presence of an external magnetic field. Fig. 5 illustrates a series of XMCD-PEEM images that were taken during a field cycle on an equilateral triangle of 2 μm edge length and 15 nm thickness from remanence to saturation. Prior to the experiment, the sample was saturated with an external field of 50 mT. The initial magnetic state for the measurement of the positive branch of the hysteresis is a flux-closure Landau state with the vortex core slightly off-center. Increasing the external field along the [100] direction pushes the vortex core out of the center along the direction of the magnetic easy axis towards the bottom edge of the triangle (0.32 mT to 0.58 mT) due to the expansion of the domain with spins parallel to the external field. At 0.71 mT the vortex core is expelled, and a clear difference in contrast can be observed between the right and left part of the triangle, which corresponds to a domain wall. Further increasing the field moves the domain wall leftwards until saturation occurs at around 1.6 mT. The same behavior was observed for the negative branch of the hysteresis loop. OOMMF simulations were carried

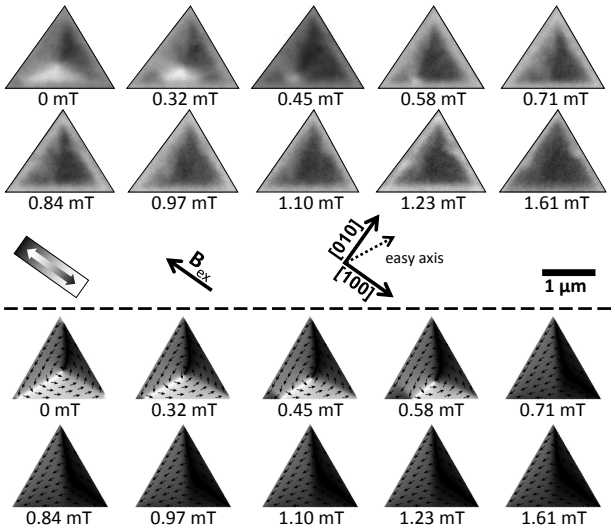

FIG. 5. Field cycle of a 2 μm sized equilateral LSMO triangle of 15 nm thickness. *Top:* XMCD-PEEM images, *bottom:* corresponding micromagnetic simulations.

out to compare the states found experimentally with the theoretically predicted ones. A relatively good agreement is observed for a magnetic easy axis direction at 27° from the [010] direction, although in the simulations the vortex is displaced along the height of the triangle. Moreover, the element magnetization does not saturate in the simulation. However, the movement of the domain wall towards the left (0.71 mT to 1.61 mT) can be reproduced. These discrepancies can be explained by thermal excitations: the PEEM images are taken at room temperature, which corresponds to almost 90% T_c, whereas the OOMMF simulations do not take temperature into account other then through the use of room temperature values for the magnetic parameters. Despite these slight discrepancies, the qualitative agreement between experiment and simulations is good, showing that the magnetic behaviour of LSMO elements can be predicted and reproduced by micromagnetic simulations, which bodes well for engineering spin structures in this material for applications.

V. CONCLUSIONS

Despite being a complex oxide, LSMO is well-suited for a large variety of applications, such as spin torque devices or magnetic tunnel junctions, since it offers a very high degree of polarization together with a magnetic state that can be controlled by the film thickness and effective magnetocrystalline anisotropy. Additionally, the magnetic state is easily reproducible and does not strongly depend on pinning. The patterning method presented here allows structuring without significantly modifying the magnetic properties.

The role of the effective magnetocrystalline anisotropy on the magnetic spin configuration of LSMO bar and triangular elements was studied using photoemission electron microscopy. We found that the dominant remanent state is a low energy flux-closure state for both thin (15 nm) and thick (50 nm) elements. The step-induced magnetic anisotropy, which competes with the dipolar energy, strongly modifies the spin configuration in the thin elements. The magnetic switching process in squares (not shown) and triangular shaped elements has also been investigated. For the latter we find a distortion of the vortex state with the vortex core moving along a direction close to the magnetic easy axis while the external magnetic field was increased along a direction close to the hard axis. The good agreement between experiment and simulation shows that the magnetic configuration of LSMO elements can be well predicted by micromagnetic simulations.

We thank Mathias Hagner for help with sample preparation. This work was supported by EU's 7th Framework Programme (IFOX NMP3-LA-2010 246102, MAGWIRE FP7-ICT-2009-5 257707), the European Research Council through the Starting Independent Researcher Grant MASPIC (ERC-2007-StG 208162), the Swiss National Science Foundation, and the German Science Foundation (DFG). Part of this work was performed at the Swiss Light Source, Paul Scherrer Institut, Villigen, Switzerland and part of this work was carried out at ELETTRA, Sincrotrone Trieste, Italy.

[1] M. Imada, A. Fujimori, and Y. Tokura, Reviews of Modern Physics **70**, 1039 (1998).
[2] Y. Tokura and Y. Tomioka, Journal of Magnetism and Magnetic Materials **200**, 1 (1999).
[3] A. Moreo, S. Yunoki, and E. Dagotto, Science **283**, 2034 (1999).
[4] Y. Tokura, Science **312**, 1481 (2006).
[5] H. Boschker, M. Huijben, A. Vailionis, J. Verbeeck, S. van Aert, M. Luysberg, S. Bals, G. van Tendeloo, E. P. Houwman, G. Koster, D. H. A. Blank, and G. Rijnders, Journal of Physics D-Applied Physics **44**, 205001 (2011).
[6] C. A. F. Vaz, J. Hoffman, C. H. Anh, and R. Ramesh, Advanced Materials **22**, 2900 (2010).
[7] H. J. A. Molegraaf, J. Hoffman, C. A. F. Vaz, S. Gariglio, D. van der Marel, C. H. Ahn, and J.-M. Triscone, Advanced Materials **21**, 3470 (2009).
[8] J. D. Burton and E. Y. Tsymbal, Physical Review B **80**, 174406 (2009).
[9] C. A. F. Vaz, J. Hoffman, Y. Segal, J. W. Reiner, R. D. Grober, Z. Zhang, C. H. Ahn, and F. J. Walker, Physical Review Letters **104**, 127202 (2010).
[10] H. Chen and S. Ismail-Beigi, Physical Review B **86**, 024433 (2012).
[11] Y. Segal, K. F. Garrity, C. A. F. Vaz, J. D. Hoffman, F. J. Walker, S. Ismail-Beigi, and C. H. Ahn, Physical Review Letters **107**, 105501 (2011).

[12] C. A. F. Vaz, M. Kläui, L. J. Heyderman, C. David, F. Nolting, and J. A. C. Bland, Physical Review B **72**, 224426 (2005).

[13] C. A. F. Vaz, M. Kläui, J. A. C. Bland, L. J. Heyderman, C. David, and F. Nolting, Nuclear Instruments & Methods in Physics Research Section B-Beam Interactions with Materials and Atoms **246**, 13 (2006).

[14] M. Kläui and C. A. F. Vaz, "Magnetisation configurations and reversal in small magnetic elements," in *Handbook of Magnetism and Advanced Magnetic Materials*, vol. 2, edited by H. Kronmüller and S. S. P. Parkin (John Wiley & Sons, 2007), p. 879.

[15] L. J. Heyderman, S. Czekaj, F. Nolting, E. Mller, P. Fischer, P. Gasser, and L. Lopez-Diaz, Journal of Applied Physics **99**, 063904 (2006).

[16] Y. Takamura, R. V. Chopdekar, A. Scholl, A. Doran, J. A. Liddle, B. Harteneck, and Y. Suzuki, Nano Letters **6**, 1287 (2006).

[17] J. Rhensius, C. A. F. Vaz, A. Bisig, S. Schweitzer, J. Heidler, H. S. Körner, A. Locatelli, M. A. Nino, M. Weigand, L. Mechin, F. Gaucher, E. Goering, L. J. Heyderman, and M. Kläui, Applied Physics Letters **99**, 062508 (2011).

[18] K. Steenbeck and R. Hiergeist, Applied Physics Letters **75**, 1778 (1999).

[19] Y. Wu, Y. Matsushita, and Y. Suzuki, Physical Review B **64**, 220404 (2001).

[20] J. Dho, Y. N. Kim, Y. S. Hwang, J. C. Kim, and N. H. Hur, Applied Physics Letters **82**, 1434 (2003).

[21] M. Kubota, T. Taniuchi, R. Yasuhara, H. Kumigashira, M. Oshima, K. Ono, H. Okazaki, T. Wakita, T. Yokoya, H. Akinaga, M. Lippmaa, M. Kawasaki, and H. Koinuma, Applied Physics Letters **91**, 182503 (2007).

[22] E. P. Houwman, G. Maris, G. M. De Luca, N. Niermann, G. Rijnders, D. H. A. Blank, and S. Speller, Physical Review B **77**, 184412 (2008).

[23] M. Ziese, Physica Status Solidi B-Basic Solid State Physics **243**, 1383 (2006).

[24] P. Perna, C. Rodrigo, E. Jimenez, F. J. Teran, N. Mikuszeit, L. Mechin, J. Camarero, and R. Miranda, Journal of Applied Physics **110**, 013919 (2011).

[25] M. J. Donahue and D. G. Porter, *OOMMF User's Guide, Version 1.0*, Interagency Report NISTIR 6376 (National Institute of Standards and Technology, Gaithersburg, MD, 1999).

[26] W. Rave and A. Hubert, IEEE Transactions on Magnetics **36**, 3886 (2000).

[27] K. J. Kirk, S. McVitie, J. N. Chapman, and C. D. W. Wilkinson, Journal of Applied Physics **89**, 7174 (2001).

[28] S. Cherifi, R. Hertel, J. Kirschner, H. Wang, R. Belkhou, A. Locatelli, S. Heun, A. Pavlovska, and E. Bauer, Journal of Applied Physics **98**, 043901 (2005).